Sensors and Actuators A 204 (2013) 37–43

Contents lists available at ScienceDirect

Sensors and Actuators A: Physical

journal homepage: www.elsevier.com/locate/sna

A multi-frequency vibration-based MEMS electromagnetic energy harvesting device

Huicong Liu [a,b,**], You Qian [b], Chengkuo Lee [b,*]

[a] Robotics and Microsystems Center, School of Mechanical & Electric Engineering, Soochow University, Suzhou 215021, PR China
[b] Department of Electrical & Computer Engineering, National University of Singapore, 4 Engineering Drive 3, Singapore 117576, Singapore

ARTICLE INFO

Article history:
Received 13 May 2013
Received in revised form 28 August 2013
Accepted 16 September 2013
Available online xxx

Keywords:
Microelectromechanical systems (MEMS)
Electromagnetic
Energy harvesting device
Multi-frequency

ABSTRACT

A multi-frequency vibration-based MEMS electromagnetic energy harvesting (EH) device has been presented, fabricated and characterized in this paper. It consists of a permanent magnet and a circular suspension structure on a MEMS EH chip. By emulating the magnetic field of a cylinder magnet, the gap distance between the magnet and EH chip is optimized to be zero for achieving larger magnetic flux change and higher output performance. From the experimental results, the vibration energy can be harvested at three excitation frequencies of 840, 1070 and 1490 Hz, which corresponds to the out-of-plane (mode I), torsion (mode II/III) and in-plane (mode IV/V) vibrations of the EH device, respectively. The maximum power densities at these three frequencies are 0.157, 0.014 and 0.117 $\mu W/cm^3$, respectively, for a matched load resistance of 626 Ω and an input acceleration of 1.0 g. The feasibility study results show promising application potentials for harvesting energy from vibrations of multi-frequency.

1. Introduction

With the growing demands of self-powered wireless sensor nodes and electronic devices, energy harvesters have been widely developed for converting ambient wasted solar [1,2], thermal [3,4] and kinetic [5–8] energy into electrical energy. Researchers have reported and reviewed various vibration-based energy harvesters based on electromagnetic [9–11], electrostatic [12], piezoelectric [13,14] and ferroelectret [15] approaches. In order to get the maximum output power, an EH device is typically designed to match its mechanical resonance with the frequency of ambient vibration source [16]. However, in practical case, the dominant frequencies of most vibration sources exhibit multiple peaks. Such examples can be found in [17,18]. A W500 Lenovo laptop exhibits two frequency peaks of 85.2 and 119 Hz, while a HVAC vent exhibits three discrete frequency peaks of 21.8, 29 and 127.3 Hz. It is therefore more effective for an EH device with multiple matched resonant frequencies.

To harvest energy from vibration sources of different frequencies, there are mainly two categories of EH solutions reported. First of all, various broadband energy harvesters have been demonstrated utilizing generator array [19], mechanical stoppers [20–22], nonlinear springs [23,24] and magnetic coupling [25–27]. But their operating frequencies are only applicable within a certain frequency range. For the second group of energy harvesters with multiple vibration modes, they are more suitable for the vibration scenarios of discrete frequency peaks. Ching et al. [28] have demonstrated an electromagnetic energy harvester with three resonant modes by using a laser-machined copper spring connected with a magnetic proof mass. Yang et al. [29] have incorporated a magnet array attached on an acrylic beam and a copper coil array to form a multi-frequency electromagnetic energy harvester. Yang et al. [30] have reported a piezoelectric energy harvester with nonlinear spring to provide vibrations of multi-frequency. Liu et al. [31] have developed a MEMS electromagnetic EH device with multiple resonant modes by using circular suspension structure. The device is able to scavenge energy from out-of-plane vibration at mode I as well as in-plane vibration at modes II and III, which would potentially be used to harvest energy from vibrations with multiple frequencies and directions. El-Hebeary et al. [32] have investigated various V-shaped and delta-shaped plates for harvesting energy from two or more closely spaced modes vibrations using electromagnetic approach.

A typical electromagnetic EH device employs fixed coils and moving magnet for increasing the transduction efficiency. The bulk magnet is assembled onto a spring structure (such as cantilever [33] or membrane [34]) to form a spring-mass oscillation system. The main problem of such MEMS prototype is that the microfabricated spring structure is very easy to be broken when conducting

* Corresponding author at: Department of Electrical & Computer Engineering, National University of Singapore, 4 Engineering Drive 3, Singapore 117576, Singapore. Tel.: +65 6516 5865; fax: +65 6779 1103.
** Corresponding author at: Robotics and Microsystems Center, Soochow University, Ganjiang East Road 178, Suzhou 215021, PR China. Tel.: +86-51267587217; fax: +86-51267587217.
E-mail addresses: bjliuhuicong@gmail.com (H. Liu), elelc@nus.edu.sg (C. Lee).

0924-4247/$ – see front matter © 2013 Elsevier B.V. All rights reserved.
http://dx.doi.org/10.1016/j.sna.2013.09.015

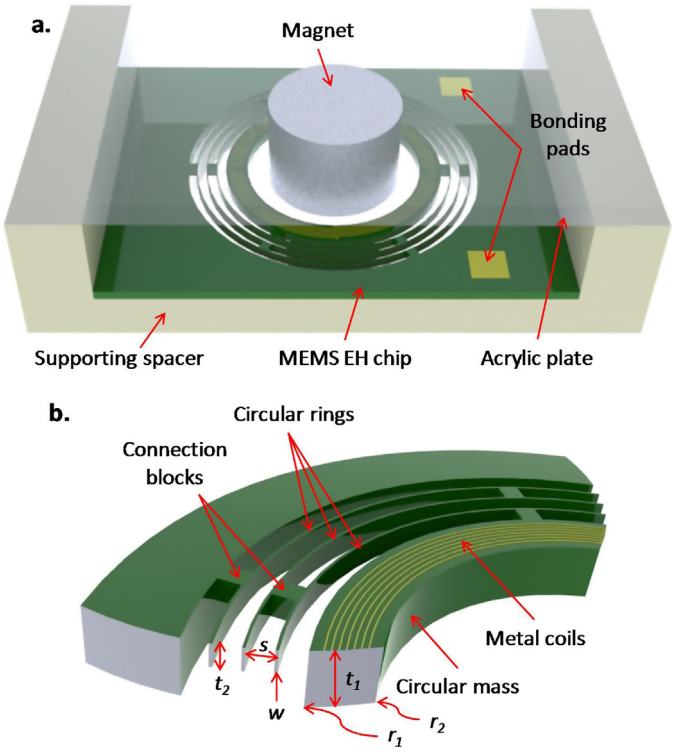

Fig. 1. Schematic drawing of the multi-frequency MEMS electromagnetic EH device.

the magnet assembly. In addition, the spring-mass structure is strongly restricted by the size and specification of the magnet. In this work, we present a multi-frequency MEMS electromagnetic EH device by using fixed magnet and moving coils. A circular suspension structure incorporated with metal coils has been retained including a circular mass and three circular rings. A bulk magnet is fixed above the suspension structure. The gap distance between the moving coils and fixed magnet can by simply adjusted by the spacer in between. Comparing with the moving magnet and fixed coils design, it has the main advantage of easy assembly. Moreover, this prototype employs a more flexible spring-mass structure for multi-frequency vibration harvesting. The resonant frequencies can be adjusted by the width, thickness and diameters of the circular spring and proof mass. In Section 2, the device design and mode analysis are presented, and the micro-fabrication process of the MEMS EH chip is described. The gap distance between the magnet and the metal coils on the circular mass has been varied and optimized in Section 3. The vibration modes of the device including out-of-plane, torsion and in-plane have been investigated and the corresponding output performance has been discussed in Section 4.

2. Device design and fabrication

Fig. 1 presents a schematic drawing of the proposed MEMS electromagnetic EH device with multiple frequencies. As shown in Fig. 1a, a MEMS EH chip of 10-mm-long, 8-mm-wide and 0.25-mm-thick is assembled on a supporting spacer. A cylindrical magnet of 2-mm-high and 1.5-mm-radius is attached on an acrylic plate and placed at the center of the circular suspension structure. Fig. 1b shows a sectional drawing of the circular suspension structure of the MEMS EH chip. The center circular mass has an outer radius r_1 of 2.5 mm and inner radius r_2 of 2 mm which allows the magnet to be placed inside the circular mass. The circular mass is suspended by three circular rings with a width w of 25 μm and each ring is linked to one another with a space s of 200 μm through a series of connection blocks at an interval of 120°. The thickness of the circular mass t_1 and circular rings t_2 are 350 μm and 100 μm, respectively. The metal coils patterned on the circular mass have two layers and each layer contains 7 winding cycles of wires of 10-μm-wide, 1-μm-thick and 40-μm-space. As the circular suspension structure of the EH device oscillates in response to the environmental vibration, the magnetic flux across the moving metal coils will be varied and thus electricity will be induced according to Faraday's law of induction.

A finite element analysis using Abaqus has been conducted to study the vibration behavior of the EH device as shown in Fig. 2. In the simulation, the dimension parameters are kept the same as the design condition. The Young's modulus of Si material is taken as 169 GPa. The first five vibration modes of the circular suspension structure are considered in the mode analysis results. At mode I of 988 Hz, the circular mass shows an out-of-plane oscillation along z-axis. At mode II of 1333 Hz and mode III of 1355 Hz, torsion vibrations of the circular suspension structure occur along x- and y-axes, respectively. The in-plane oscillations appear at mode IV of 1494 Hz and mode V of 1513 Hz along x- and y-axes, respectively. It is because of the symmetric configuration of the circular suspension structure that the frequencies at torsion modes II and III are almost similar, while the frequencies at in-plane modes IV and V are approximately the same.

Fig. 3 shows the fabrication processes of the MEMS EH chip, which starts from a silicon on insulator (SOI) wafer of 100-μm-thick Si device layer, 1-μm-thick buried oxide layer and 250-μm-thick Si handling layer. In Fig. 3a, a 0.1-μm-thick Si_3N_4 insulating layer and 1-μm-thick Al metal layer are firstly deposited on the frontside surface by plasma-enhanced chemical vapor deposition (PECVD) and physical vapor deposition (PVD), respectively. The first winding coil layer is patterned by reactive ion etching (RIE) through mask 1 and then a 0.8-μm-thick PECVD Si_3N_4 insulating layer is deposited and etched to form the via openings through mask 2. In Fig. 3b, a 1-μm-thick Al coil layer and 0.8-μm-thick PECVD Si_3N_4 insulating layer are similarly deposited and patterned to form the second winding coil layer and opening pads through masks 3 and 4. In Fig. 3c, a 2-μm-thick PECVD SiO_2 is deposited and etched as a passivating layer through mask 5. It is followed by a series of frontside RIE and deep RIE (DRIE) processes to create the circular suspension structure of the EH chip. In Fig. 3d, a backside DRIE process is conducted by using the patterned photo resist and 2-μm-thick SiO_2 layer through mask 6. Finally, a CHF_3 plasma etching process is performed to eventually remove the remaining SiO_2 layers and release the suspension structure as shown in Fig. 3e. Fig. 4 shows a photograph of the micro-fabricated EH chip assembled onto a dual in-line package (DIP). The enlarged views of parts A and B by microscope are shown in figure. It is observed that during the frontside DRIE process, the width of the circular ring is over-etched from 25 μm to approximately 20 μm. Such geometrical variation leads to the change of the resonant frequencies of the EH device.

3. Magnetic field analysis

According to Faraday's law of induction, the induced voltage of metal coils is proportional to the negative of the rate of change of the magnetic flux across the closed-loop coils:

$$\varepsilon = -\frac{d\Phi}{dt} = -\frac{d}{dt}\sum_{i=1}^{n}(\vec{B}_i \cdot \vec{S}_i) \quad (1)$$

where Φ is the magnetic flux; t is the time; n is the total circles of the winding coils; i is the circle order; B_i is the magnetic field in the i-th circle and S_i is the area included in the i-th circle. As the multi-frequency electromagnetic EH device resonates at out-of-plane, torsion or in-plane modes, the change of the magnetic

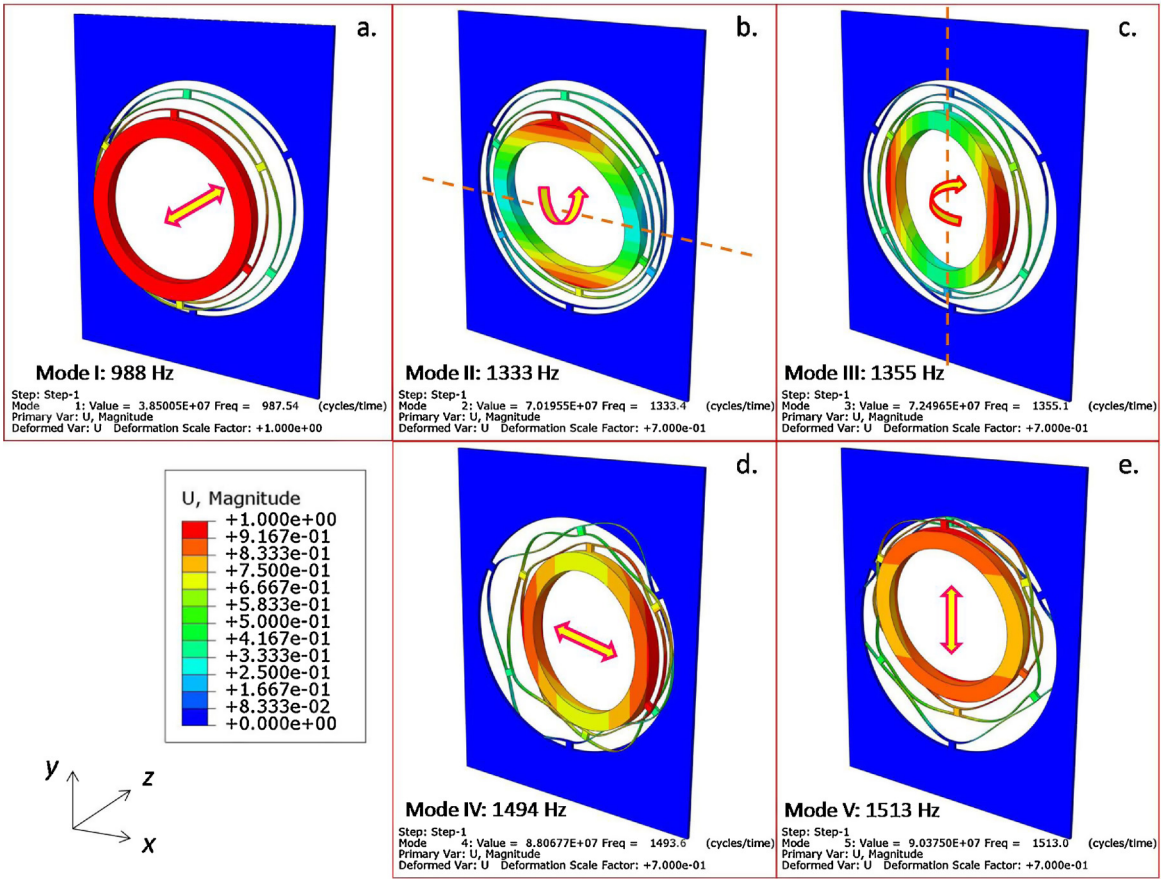

Fig. 2. Finite element analysis results: (a) mode I at 988 Hz; (b) mode II at 1333 Hz; (c) mode III at 1355 Hz; (d) mode IV at 1494 Hz and (e) mode V at 1513 Hz.

flux across the coils will induce electric voltage. In order to experience the maximum magnetic flux change of the winding coils and eventually achieve the maximum induced voltage, it is essential to analyze the magnetic field of the cylinder magnet and optimize the position between the magnet and coils. The distribution of the magnetic field of a permanent cylinder magnet can be calculated using magnetic scalar potential [35], which is given by a triple integral in cylindrical coordinate as:

$$\Phi(\rho,z)=\frac{\mu_0}{4\pi}M\iiint\frac{(z-Z)RdRd\varphi dZ}{\left[\rho^2-2R\rho\cos\varphi+R^2+(z-Z)^2\right]^{3/2}}=\frac{\mu_0}{4\pi}M\times\left(\iint\frac{RdRd\varphi}{\sqrt{\rho^2-2R\rho\cos\varphi+R^2+(L/2-z)^2}}-\iint\frac{RdRd\varphi}{\sqrt{\rho^2-2R\rho\cos\varphi+R^2+(L/2+z)^2}}\right)\quad(2)$$

where it can be interpreted as originating from two parallel oppositely charged monopolar disks of radius r separated by a perpendicular distance L; M is the saturation magnetization and μ_0 is the permeability of vacuum ($\mu_0 M = 1.61$ T); R, φ and Z are the three variables in the cylindrical coordinate; (ρ, z) represents an arbitrary point in a 2-dimentional (2-D) section plane through the center axis of the cylindrical magnet. By doing the numerical computations, the magnetic field components of $B_\rho = -\partial\Phi/\partial\rho$ and $B_Z = -\partial\Phi/\partial z$ are given in double integrals as:

$$B_\rho=-\frac{\mu_0}{4\pi}M\int_0^{2\pi}\int_0^{r}\left(\frac{R(2\rho-2R\cos\varphi)}{2(R^2+(L/2+z)^2+\rho^2-2R\rho\cos\varphi)^{3/2}}-\frac{R(2\rho-2R\cos\varphi)}{2(R^2+(L/2-z)^2+\rho^2-2R\rho\cos\varphi)^{3/2}}\right)dRd\varphi\quad(3)$$

$$B_z=-\frac{\mu_0}{4\pi}M\int_0^{2\pi}\int_0^{r}\left(\frac{R(L/2+z)}{(R^2+(L/2+z)^2+\rho^2-2R\rho\cos\varphi)^{3/2}}-\frac{R(L/2-z)}{(R^2+(L/2-z)^2+\rho^2-2R\rho\cos\varphi)^{3/2}}\right)dRd\varphi\quad(4)$$

From Eqs. (3) and (4), the magnetic field components B_ρ and B_z can be obtained for any specific position (ρ, z) in a 2-D section plane through the center axis of a cylindrical magnet. As shown in Fig. 5a, the magnetic field vector B around a cylinder magnet of 2-mm-height and 1.5-mm-radius is represented in blue arrows in view of the magnitude and direction. ρ and z are the horizontal and vertical displacements to the center O of the magnet. The circular mass is positioned below the magnet center with a variable vertical displacement from 0 to −1.5 (-1.5 < z < 0) mm, while the metal coils on the circular mass is in between the horizontal displacements of 2 to 2.5 ($2 < \rho < 2.5$) mm and −2.5 to −2 ($-2.5 < \rho < -2$) mm. Fig. 5b shows the magnetic field component B_z (in blue) and the change of the magnetic field ΔB_z (in red) versus different vertical

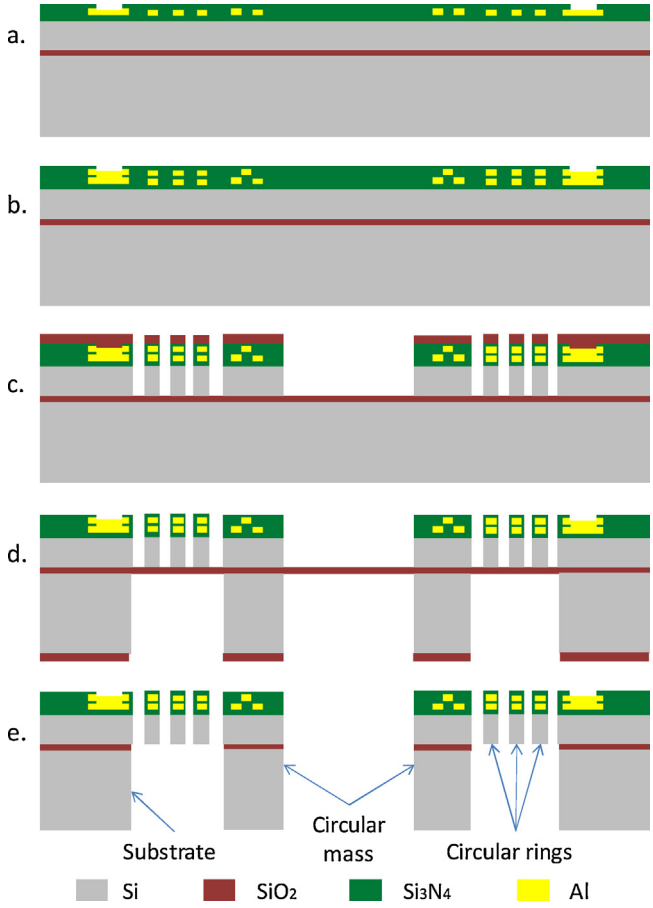

Fig. 3. Micro-fabrication processes of the EH chip.

displacements for a fixed horizontal displacement $\rho = 2$ mm (line A–A′). It is seen from the figure that the maximum change of the magnetic field ΔB_z occurs at the vertical displacements of $z = -1$ and $z = 1$ mm. As the circular mass is positioned at $z = -1$ mm, which means the gap distance between the circular mass and the magnet is zero, the winding coils would experience a maximum change of magnetic flux and subsequently induce a maximum voltage output. Such trend has been verified to be similar for any circle of winding coils in between horizontal displacements of 2 to 2.5 mm and −2.5 to −2 mm.

In the case that the winding coils experience a peak-to-peak vibration displacement of about 0.12 mm, the maximum and minimum vertical displacements are z_max of −0.94 mm and z_min of −1.06 mm, respectively, with respect to the initial position $z\_initial$ of −1 mm. According to Eq. (4), the magnetic field component Bz against different horizontal displacement can be calculated at $z\_max = -0.94$ and $z\_min = -1.06$ mm as shown in Fig. 6. The change of the magnetic field Bz_delta for the peak-to-peak vibration displacement of the moving coils experienced is plotted in the same figure by subtracting the magnetic field component Bz at z_max from that at z_min. It is found that for the winding coils located from −2.5 to −2 mm (indicated in shadow C) and from 2 to 2.5 mm (indicated in shadow C′) experience a maximum change of magnetic field Bz_delta from 0.118 to 0.164 T.

4. Dynamic characterization

In the experiment, the multi-frequency EH device is mounted on a vibration shaker. A dynamic signal analyzer is used to generate a sweep-sine signal in a frequency range or a single sinusoidal signal at a specific frequency to the shaker through an amplifier. The output voltage of the EH device is collected to the dynamic signal analyzer. At an input acceleration of 1.0 g, Fig. 7 shows the various output voltages of the device at mode I of 840 Hz, as the vertical displacement of top surface of the circular mass changes from

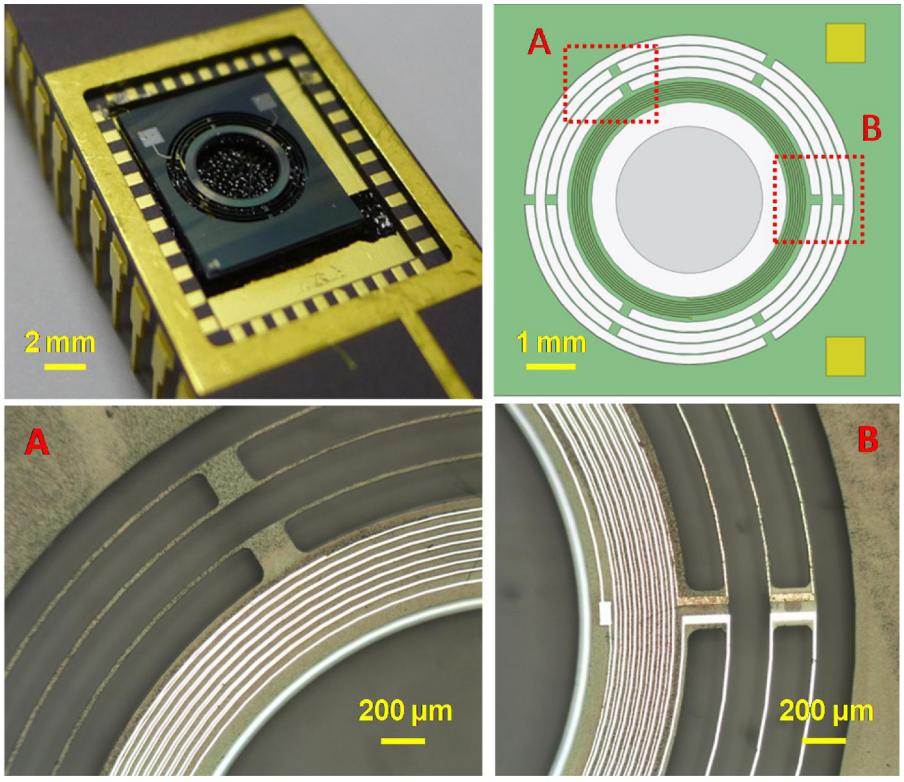

Fig. 4. (a) Photograph of the micro-fabricated EH chip assembled onto a DIP; (b) enlarged views of parts A and B of the EH chip taken by microscope.

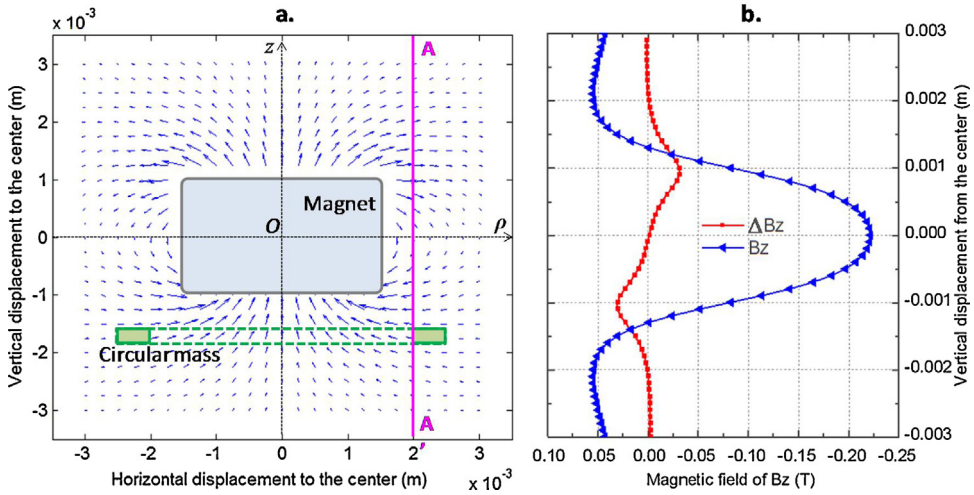

Fig. 5. (a) Magnetic field distribution around a cylinder magnet of 2-mm-height and 1.5-mm-radius; (b) magnetic field component B_z and magnetic field change ΔB_z against the vertical displacement for a fixed horizontal displacement of 2 mm.

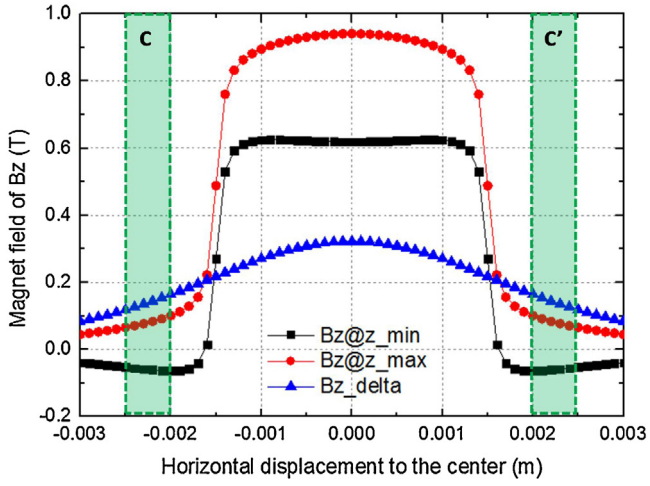

Fig. 6. Magnetic field component *Bz* and the change of the magnetic field *Bz*_delta for the peak-to-peak vibration displacement of the moving coils experienced.

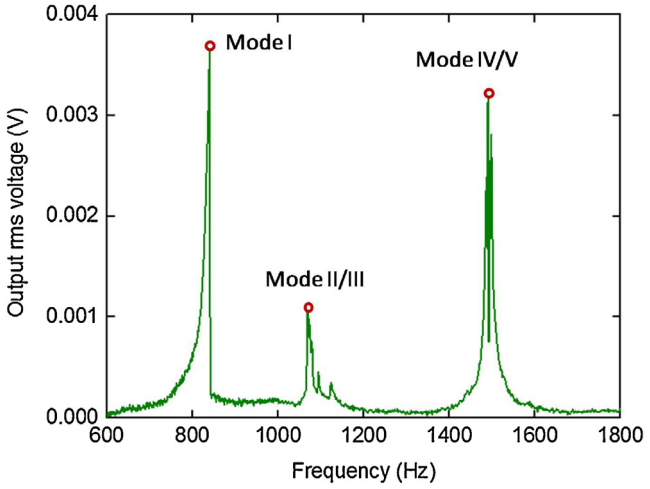

Fig. 8. Output voltage of the EH device against the excitation frequency sweeping from 600 to 1800 Hz at 1.0 g.

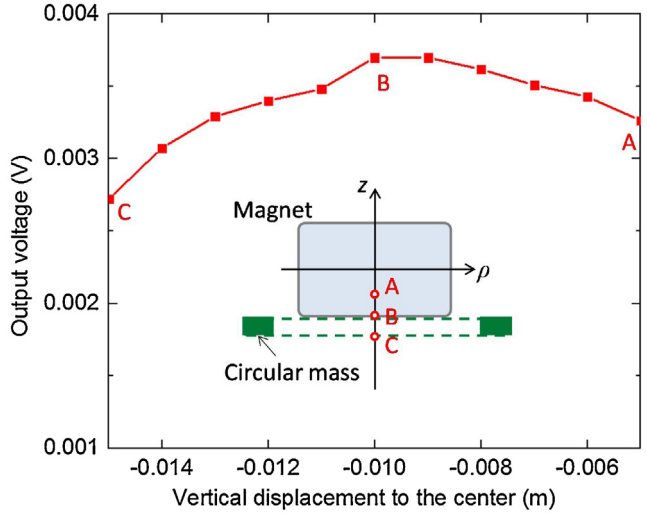

Fig. 7. Output voltage of the EH device against the vertical displacement of the circular mass from −0.5 to −1.5 mm at vibration mode I.

−0.5 mm (point A), −1 mm (point B) to −1.5 mm (point C) at a shift step of 0.1 mm. It is clearly seen that the maximum voltage output of 0.0037 V is introduced through the winding coils as the top surface of the circular mass is at point B (i.e. zero gap distance), which agrees well with the theoretical result in Fig. 5b. When the vertical displacement of the top surface of the circular mass changes step by step from −1 to −0.5 mm, the output voltage decreases gradually to 0.0027 V at point A. Similarly, the output voltage shows a slightly decreasing trend until 0.0033 V at point C as the vertical displacement of the top surface of the circular mass varies gradually from −1 to −1.5 mm. Therefore, the position of the circular mass with winding coils patterned on the top surface is fixed at point B (i.e. vertical displacement of −1 mm) in the later dynamic test for the sake of optimal output performance.

At the same input acceleration of 1.0 g, the output voltage of the EH device against the excitation frequency sweeping from 600 to 1800 Hz is shown in Fig. 8. Three voltage peaks of 0.0037, 0.0011 and 0.0032 V are found at resonant frequencies of 840, 1070 and 1490 Hz, respectively. Based on the mode analysis results shown in Fig. 2, these three frequencies actually correspond to the out-of-plane (mode I), torsion (mode II/III) and in-plane (mode IV/V) resonant modes, respectively. For the torsion modes II and III, it is seen only one frequency peak at 1070 Hz. It could be because

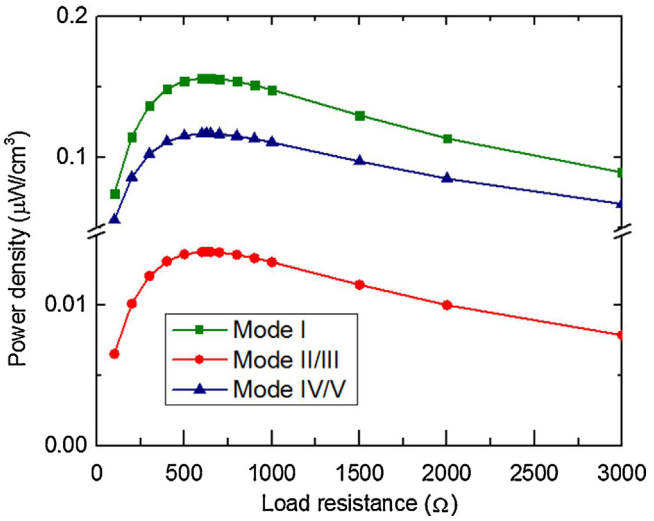

Fig. 9. Output power density versus various load resistances for the three vibration frequencies of 840 (mode I), 1070 (mode II/III) and 1490 (mode IV/V) Hz.

the frequency difference between modes II and III is only 22 Hz in the simulation. It is hard to distinguish these two related torsion frequencies in the voltage response trace. Similarly, it is too close to make a distinction between the two in-plane modes IV and V, since the frequency difference is only 19 Hz. Hence, there is only one frequency peak at 1490 Hz for in-plane modes IV and V. For the resonance differences between simulation and experimental results, it is mainly due to the geometrical variation of the circular rings during the frontside DRIE process. The internal resistance of the winding coils of two layers is 626 Ω. As the load resistance is equal to the internal coil resistance, the optimal power output of 5.5, 0.5 and 4.1 nW at the respective resonant frequencies of 840, 1070 and 1490 Hz can be achieved. Fig. 9 shows the output power density versus various load resistances for the three vibration modes, where the power density is obtained from the output power divided by the device volume of 0.035 cm^3 (chip volume of 0.02 cm^3 and magnet volume of 0.015 cm^3). It is found the maximum power densities of modes I, II/III and IV/V are 0.157, 0.014 and 0.117 $\mu W/cm^3$, respectively, under a matched load resistance of 626 Ω.

5. Conclusion

In this paper, we have proposed and fabricated a vibration-based MEMS electromagnetic EH device with multiple frequencies. For attaining a good output performance, the magnetic field surrounding the cylinder magnet is analyzed, and the position between the magnet and the EH chip is optimized to be zero gap distance. From experimental results, the vibration energy under the three excitation frequencies of 840 (mode I), 1070 (mode II/III) and 1490 (mode IV/V) Hz have been investigated. At an input acceleration of 1.0 g, the corresponding optimal power densities at these three frequencies are 0.157, 0.014 and 0.117 $\mu W/cm^3$, respectively, for a matched load resistance of 626 Ω. With further increment of the circular mass area, winding coils and softening of the circular spring, the proposed EH device could harvest more energy from vibration sources of multiple frequencies.

Acknowledgements

This work is partially supported by Faculty Research Committee (FRC) Grant (R-263-000-692-112) at the National University of Singapore (NUS), and the NRF-CRP001-057 Program "Self-powered body sensor network for disease management and prevention-oriented healthcare" under R-263-000-A27-281 from National Research Foundation (NRF), Singapore.

References

[1] B. Oregan, M. Gratzel, A low-cost, high-efficiency solar cell based on dye-sensitized colloidal TiO_2 films, Nature 353 (6346) (1991) 737–740.
[2] M. Law, L.E. Greene, J.C. Johnson, R. Saykally, P. Yang, Nanowire dye-sensitized solar cells, Nat. Mater. 4 (6) (2005) 455–459.
[3] J. Xie, C. Lee, H. Feng, Design, fabrication, and characterization of CMOS MEMS-based thermoelectric power generators, J. Microelectromech. Syst. 19 (2) (2010) 317–324.
[4] J. Xie, C. Lee, M.F. Wang, Y. Liu, H. Feng, Characterization of heavily doped polysilicon films for CMOS-MEMS thermoelectric power generators, J. Micromech. Microeng. 19 (12) (2009) 125029.
[5] S. Roundy, P.K. Wright, A piezoelectric vibration based generator for wireless electronics, Smart Mater. Struct. 13 (5) (2004) 1131–1142.
[6] A. Khaligh, P. Zeng, C. Zheng, Kinetic energy harvesting using piezoelectric and electromagnetic technologies – state of the art, IEEE Trans. Ind. Electron. 57 (3) (2010) 850–860.
[7] H. Liu, S. Zhang, R. Kathiresan, T. Kobayashi, C. Lee, Development of piezoelectric microcantilever flow sensor with wind-driven energy harvesting capability, Appl. Phys. Lett. 100 (22) (2012) 223905.
[8] H. Liu, C. Lee, T. Kobayashi, C.J. Tay, C. Quan, Piezoelectric MEMS-based wide-band energy harvesting systems using a frequency-up-conversion cantilever stopper, Sens. Actuators A: Phys. 186 (2012) 242–248.
[9] D.P. Arnold, Review of microscale magnetic power generation, IEEE Trans. Magn. 43 (11) (2007) 3940–3951.
[10] S. Roundy, E. Takahashi, A planar electromagnetic energy harvesting transducer using a multi-pole magnetic plate, Sens. Actuators A: Phys. 195 (2013) 98–104.
[11] K. Ashraf, M.H. Md Khir, J.O. Dennis, Z. Baharudin, Improved energy harvesting from low frequency vibrations by resonance amplification at multiple frequencies, Sens. Actuators A: Phys. 195 (2013) 123–132.
[12] Y. Suzuki, Recent progress in MEMS electret generator for energy harvesting, IEEJ Trans. Electr. Electr. Eng. 6 (2) (2011) 101–111.
[13] S. Saadon, O. Sidek, A review of vibration-based MEMS piezoelectric energy harvesters, Energy Convers. Manage. 52 (1) (2011) 500–504.
[14] N. Heidrich, F. Knöbber, V. Polyakov, V. Cimalla, W. Pletschen, R.E. Sah, L. Kirste, S. Leopold, S. Hampl, O. Ambacher, V. Lebedev, Corrugated piezoelectric membranes for energy harvesting from aperiodic vibrations, Sens. Actuators A: Phys. 195 (2013) 32–37.
[15] Y. Feng, K. Hagiwara, Y. Iguchi, Y. Suzuki, Trench-filled cellular parylene electret for piezoelectric transducer, Appl. Phys. Lett. 100 (2012) 262901.
[16] P.D. Mitcheson, T.C. Green, E.M. Yeat, H.S. Holmes, Architectures for vibration-driven micropower generators, J. Microelectromech. Syst. 13 (3) (2004) 429–440.
[17] E. Reilly, L. Miller, R. Fain, P.K. Wright, A study of ambient vibrations for piezoelectric energy conversion, Proc. PowerMEMS 2009 (2009) 312–315.
[18] L.M. Miller, E. Halvorsen, T. Dong, P.K. Wright, Modeling and experimental verification of low-frequency MEMS energy harvesting from ambient vibrations, J. Micromech. Microeng. 21 (4) (2011) 045029.
[19] I. Sari, T. Balkan, H. Kulah, An electromagnetic micro power generator for wideband environmental vibrations, Sens. Actuators A 123 (124) (2008) 63–72.
[20] H. Liu, C.J. Tay, C. Quan, T. Kobayashi, C. Lee, M.E.M.S. Piezoelectric, energy harvester for low-frequency vibrations with wideband operation range and steadily increased output power, J. Microelectromech. Syst. 20 (5) (2011) 1131–1142.
[21] H. Liu, C. Lee, T. Kobayashi, C.J. Tay, C. Quan, Investigation of a MEMS piezoelectric energy harvester system with a frequency-widened-bandwidth mechanism introduced by mechanical stoppers, Smart Mater. Struct. 21 (3) (2012) 035005.
[22] H. Liu, C. Lee, T. Kobayashi, C.J. Tay, C. Quan, A new S-shaped MEMS PZT cantilever for energy harvesting from low frequency vibrations below 30 Hz, Microsyst. Technol. 18 (4) (2012) 497–506.
[23] D.S. Nguyen, E. Halvorsen, Nonlinear springs for bandwidth-tolerant vibration energy harvesting, J. Microelectromech. Syst. 20 (6) (2011) 1225–1227.
[24] L. Tang, Y. Yang, A nonlinear piezoelectric energy harvester with magnetic oscillator, Appl. Phys. Lett. 101 (9) (2012) 094102.
[25] T. Galchev, E. Aktakka, K. Najafi, A piezoelectric parametric frequency increased generator for harvesting low-frequency vibrations, J. Microelectromech. Syst. 21 (2012) 1311–1320.
[26] Y. Uzun, E. Kurt, The effect of periodic magnetic force on a piezoelectric energy harvester, Sens. Actuators A: Phys. 192 (2013) 58–68.
[27] I.N. Ayala-Garcia, P.D. Mitcheson, E.M. Yeatman, D. Zhu, J. Tudor, S.P. Beeby, Magnetic tuning of a kinetic energy harvester using variable reluctance, Sens. Actuators A: Phys. 189 (2013) 266–275.
[28] N.N.H. Ching, H.Y. Wong, W.J. Li, P.H.W. Leong, Z. Wen, A laser-micromachined multi-modal resonating power transducer for wireless sensing systems, Sens. Actuators A: Phys. 97-98 (2002) 685–690.

[29] B. Yang, C. Lee, W. Xiang, J. Xie, J.H. He, R.K. Kotlanka, S.P. Low, H. Feng, Electromagnetic energy harvesting from vibrations of multiple frequencies, J. Micromech. Microeng. 19 (3) (2009) 035001.
[30] B. Yang, J. Liu, G. Tang, J. Luo, C. Yang, Y. Li, A generator with nonlinear spring oscillator to provide vibrations of multi-frequency, Appl. Phys. Lett. 99 (22) (2012) 223505.
[31] H. Liu, B.W. Soon, N. Wang, C.J. Tay, C. Quan, C. Lee, Feasibility study of a 3-D vibration-driven electromagnetic MEMS energy harvester with multiple vibration modes, J. Micromech. Microeng. 22 (12) (2012) 125020.
[32] M.M.R. El-Hebeary, M.H. Arafa, S.M. Megahed, Modeling and experimental verification of multi-modal vibration energy harvesting from plate structures, Sens. Actuators A: Phys. 193 (2013) 35–47.
[33] S.P. Beeby, R.N. Torah, M.J. Tudor, P. Glynne-Jones, T. O'Donnell, C.R. Saha, S. Roy, J. Micromech. Microeng. 17 (7) (2007) 1257–1265.
[34] C. Shearwood, R.B. Yates, Development of an electromagnetic microgenerator, Electron. Lett. 33 (22) (1997) 1883–1884.
[35] H.A. Haus, J.R. Melcher, Electromagnetic Fields and Energy (MIT OpenCourseWare), http://web.mit.edu/6.013_book/www/

Biographies

Huicong Liu received her B.Eng. and M.Sc. degrees in Department of Mechanical Engineering from University of Science and Technology Beijing, China, in 2006 and 2008 respectively. She received her Ph.D. degree from the Department of Mechanical Engineering, National University of Singapore (NUS) in Jan. 2013. She has been a Research Fellow in Department of Electrical and Computer Engineering, NUS from Aug. 2012 to Aug. 2013. Currently she is an associate professor in Robotics and Microsystems Center, School of Mechanical & Electric Engineering, Soochow University, China. Her research interests are vibration-based MEMS energy harvesters and self-powered MEMS devices.

You Qian received his B.Eng. degree from the School of Microelectronics and Solid-state Electronics at the University of Electronic Science and Technology of China (UESTC), Chengdu, China, in 2009 and M.Sc. degree from Department of Electrical and Computer Engineering at National University of Singapore in 2010. He is now a Research Engineer at ECE, NUS and pursuing his doctorate degree in the same department. He is also currently attached to Institute of Microelectronics (IME), A*STAR. His research interests are focused on NEMS switches.

Chengkuo Lee received the M.S. degree in materials science and engineering from National Tsing Hua University, Hsinchu, Taiwan, in 1991, the M.S. degree in industrial and system engineering from Rutgers University, New Brunswick, NJ, in 1993, and the Ph.D. degree in precision engineering from The University of Tokyo, Tokyo, Japan, in 1996. He worked as a Foreign Researcher in the Nanometerscale Manufacturing Science Laboratory of the Research Center for Advanced Science and Technology, The University of Tokyo, from 1993 to 1996. He had also worked in the Mechanical Engineering Laboratory, AIST, MITI of Japan as a JST Research Fellow in 1996. Thereafter, he became a Senior Research Staff Member of the Microsystems Laboratory, Industrial Technology Research Institute, Hsinchu, Taiwan. In September 1997, he joined Metrodyne Microsystem Corporation, Hsinchu, Taiwan, and established the MEMS device division and the first micromachining fab for commercial purposes in Taiwan. He was the Manager of the MEMS device division between 1997 and 2000. He was an Adjunct Assistant Professor in the Electro-physics Department of National Chiao Tung University, Hsinchu, Taiwan, in 1998, and an Adjunct Assistant Professor in the Institute of Precision Engineering of National Chung Hsing University, Taichung, Taiwan, from 2001to 2005. In August 2001, he cofounded Asia Pacific Microsystems, Inc. (APM), where he first became Vice President of R&D, before becoming Vice President of the optical communication business unit and Special Assistant to the Chief Executive Officer in charge of international business and technical marketing for the MEMS foundry service. From 2006 to 2009, he was a Senior Member of the Technical Staff at the Institute of Microelectronics, A-Star, Singapore. Currently he is an associate Professor in the Department of Electrical and Computer Engineering, National University of Singapore, Singapore. He is the coauthor of Advanced MEMS Packaging (McGraw-Hill, 2010). He has contributed to more than 190 international conference papers and extended abstracts and 130 peer-reviewed international journal articles in the fields of Sensors, Actuators, Energy Harvesting, MEMS, NEMS, nanophotonics, and nanotechnology. He is also the holder of nine U.S. patents.